Proceedings of the ASME 2021 Gas Turbine India Conference
GTINDIA2021
December 2 – 3, 2021 (Virtual Conference, Online)

GTIndia2021-75990

ESTIMATING THE AERODYNAMIC COEFFICIENTS OF A SAVONIUS ROTOR BLADE PROFILE DEVELOPED THROUGH THE SIMPLEX SEARCH METHOD

Man Mohan
PhD Student
Department of Mechanical Engineering
Indian Institute of Technology Guwahati
Guwahati- 781039, Assam, India

Divyeshkumar D. Kansagara
MTech Student
Department of Mechanical Engineering
Indian Institute of Technology Guwahati
Guwahati – 781039, Assam, India.

Deepak Sharma
Associate Professor
Department of Mechanical Engineering
Indian Institute of Technology Guwahati
Guwahati – 781039, Assam, India.

Ujjwal K. Saha*
Professor
Department of Mechanical Engineering
Indian Institute of Technology Guwahati
Guwahati – 781039, Assam, India.

ABSTRACT

The Savonius rotor, a type of vertical-axis wind turbine, seems to be promising for small-scale power generation. Most of the studies conducted so far have focused on the evaluation of torque and power coefficients (C_T, C_P) of the rotor. This paper aims at analyzing the aerodynamic drag and lift coefficients (C_D, C_L) of a Savonius rotor blade profile that is generated by the simplex search method to maximize its C_P. The optimization is carried out by coupling the numerical simulations with the simplex search method. The optimized blade profile thus obtained is symmetric about its axis, where one half is created through a natural cubic spline curve using three points. Two-dimensional (2D) unsteady numerical simulations have been conducted by adopting ANSYS FLUENT solver to examine the C_D and C_L of the optimized blade profile at an inlet air velocity of 7.30 m/s. The shear stress transport (SST) k-ω turbulence model is used to solve the transient Reynolds-averaged Navier-Stokes (RANS) equations. The aerodynamic analysis is performed over a range of tip speed ratios (TSRs). The total pressure, velocity magnitudes, and the turbulent intensity contours of the optimized blade profile are generated and studied at different angles of rotation. The C_D and C_L of the blade profile are investigated for a complete rotation with an increment of 1°. At TSR = 0.8, the optimized profile shows a C_{Dmax} of 1.91 at an angle of rotation of 54°, while C_{Dmin} is found to be 0.45 at an angle 147°.

Keywords: Savonius rotor; Blade profiles; Lift and drag coefficients, Power coefficient; Tip-speed ratio; CFD simulations; Simplex search technique.

*Corresponding author
Email: saha@iitg.ernet.in
Tel: 0091-361-2582663: Fax: 0091-361-2690762

NOMENCLATURE

A	Swept area	[m^2]
AR	Aspect ratio	--
CFD	Computational Fluid Dynamics	--
C_D	Drag coefficient	--
C_L	Lift coefficient	--
C_P	Power coefficient	--
C_T	Torque coefficient	--
D	Diameter of rotor	[m]
d	Chord length of the blade profile	[m]
F_L	Lift force	[N]
F_D	Drag force	[N]
H	Rotor height	[m]
N	Rotational speed of a rotor	[rpm]
OR	Overlap Ratio	--
L	Radius of the blade profile	[m]
RANS	Reynolds-averaged Navier-Stokes	--
RPM	Revolution per minute	--
SG	Separation gap	--
SST	Shear Stress Transport	--
TSR	Tip Speed Ratio	--
u	Rotor speed	[m/s]
V	Free stream wind velocity	[m/s]
VAWT	Vertical-axis Wind Turbine	--

Greek Symbols

ρ	Density of air	[kg/m^3]
α	Angle of attack	[degree]
k	Turbulent kinetic energy	[m^2/s^2]
ε	Turbulence dissipation rate	[m^2/s^3]
ω	Rotational speed of rotor	[rad/s]

1 INTRODUCTION

The need for energy is changing the way civilization is changing. In recent times, demand for energy has been largely determined by the burning of fossil fuels. Moreover, the usage of fossil fuels leads to various hazardous results like global warming, pollution, health issues, and others [1]. Therefore, this is the right time to switch the dependence on fossil fuels. Thereby, shifting to renewable energy is a worthy idea. One of the renewable sources of energy could be wind energy which can deal with the energy crisis that the world is facing [2]. Wind turbines are the device used to transform wind energy into electrical energy. Depending on the axis of rotation, the wind turbines are classified into horizontal-axis wind turbines (HAWTs) and vertical-axis wind turbine (VAWTs). Presently, the VAWTs, such as Savonius and Darrieus rotors, are gaining a lot of popularity in reaping the power from the incoming air at a small-scale. Apart from this, a VAWT has got various advantages such as low cost of production, independence on the wind direction, ease of maintenance, roof solution for domestic energy demand, and others. Moreover, the Savonius rotor is characterized by its self-staring capability, and gives an efficiency of around 30% as reported in the open literature [3]. However, a minimal amount of lift force is also appreciated in power production [4]. Since the Savonius rotors are compact in design, therefore they could be installed even in small regions and can be used for pumping, farming, and others. The geometric briefings of a semicircular rotor are displayed in Figure 1.

The conventional Savonius rotor suffers from low productivity, and therefore, continuous efforts are being made during the last four decades to improve its performance. In this regard, several investigations focusing into the aspect ratio (*H/2L*), overlap ratio (*e/L*), end plates, number of blades, nature of profiles, twist angle, rotor staging, and other parameters [5-8]. Since the Savonius rotor works on lift and drag forces (F_L, F_D), these forces are directly a function of aerodynamic coefficients, density of air, area of the rotor blade, and the relative air velocity of the rotor blade (difference between the wind speed and the rotor surface speed, $u = r\omega$) [9]. Figure 2 shows the F_D and F_L acting on the rotor blade. The drag and lift coefficients (C_D and C_L) can be denoted by the equations (1) and (2), respectively [9,10].

$$C_D = \frac{F_D}{\frac{1}{2}\rho A(V-u)^2} \quad (1)$$

$$C_L = \frac{F_L}{\frac{1}{2}\rho A(V-u)^2} \quad (2)$$

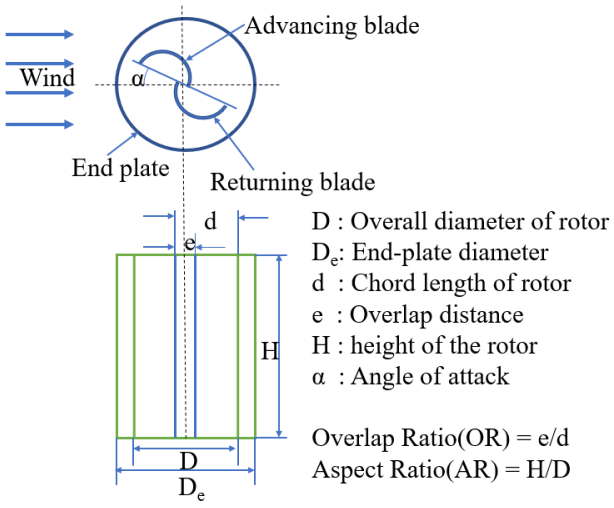

Figure 1: Geometric details of a Savonius rotor

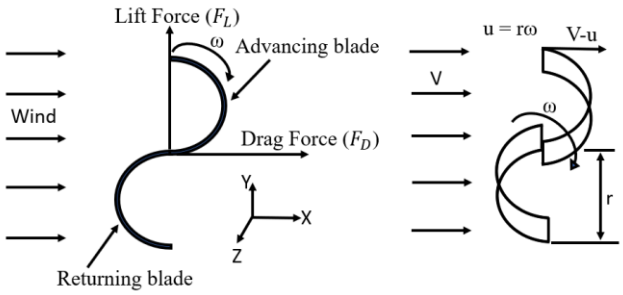

Figure 2: Lift force, drag force, and relative wind velocity

A very little research on the drag and lift forces has been noticed so far, which is confined to some selected blade profiles only. In 1989, Chauvin and Benghrib [11] were the first to analyse the impact of C_L and C_D on the conventional blade by creating the pressure drop amid the top and bottom surfaces of the rotor blade. A negative amount of C_L is present at a lesser amount of *TSR*. However, the C_L becomes positive with an increase in *TSR*. Thereafter, for nearly a couple of decagons, there was a draught on the study of C_L and C_D attributes of such a rotor. Later, Irabu and Roy [12] had investigated experimentally and demonstrated that the highest C_D of the traditional rotor blade to be 1.56 at $\alpha = 90^o$ and 270^o at an *OR* = 0.0. The C_D was found to decrease with the increase in the *OR*. The maximum and minimum C_L is found to be 0.6 and 0.2 at *OR* of 0.0 and 1.0, respectively. Jaohindy et al. [13] had scrutinized the outcome of C_D and C_L numerics for the conventional rotor blade, where the C_{Dmax} was found to be 2.2 in the range of $\alpha = 60^o$-70^o at *TSR* = 0.6. The C_{Lmax} is about 1.72 at $\alpha = 30^o$ and 210^o without altering *TSR* values. At a later stage, Roy and Ducoin [14] executed 2D unsteady simulations to investigate the C_D and C_L of a new blade profile. They found the C_{Dmax} for the Roy profile to be 2.24 at $\alpha = 80^o$. For the Roy profile at *TSR* = 0.60, the C_{Lmax} obtained is 2.07. The analysis of C_D and C_L was initially done basically for conventional semicircular blade profile.

In recent times, analysis on C_D and C_L was performed for the modified Bach and Benesh profiles by Alom et al. [15]. A 2D unsteady simulation was carried out by them at *TSR* = 0.6 to investigate the C_{Dmax} of the modified Bach profile. It was noted that C_{Dmax} is 2.31 at $\alpha = 96^o$ and 276^o. The C_{Dmax} obtained for the Benesh profile was 1.98 and 2.01 at $\alpha = 75^o$ and 256^o, respectively. The C_{Lavg} for modified Bach, Benesh, and semicircular profiles were 0.95, 1.32, and 0.96, respectively. The C_{Lmax} obtained for modified Bach was around 1.97 at $\alpha = 30^o$ and 210^o, considering that for Benesh profile $C_{Dmax} = 2.25$ ($\alpha = 15^o$) and $C_{Lmax} = 2.21$ ($\alpha = 196^o$). It is thus evident that the analysis of C_D and C_L is confided up to few profiles only. In recent times, newer blade profiles have been developed through the optimization techniques. It is thus necessary to analyze the C_D and C_L values of the blade profiles that is generated through the optimization procedure. In a previous study [16], a blade profile is developed by simplex search method where the power coefficient (C_P) is taken as an output function. However, the aerodynamic behavior of this optimized profile is not studied so far. In view of this, the present study aims at analyzing the aerodynamic coefficients of the optimized profile.

Most of studies related to the Savonius rotors dealt with the performance parameters like torque and power coefficients (C_T, C_P) [5-8]. As mentioned earlier, the study of C_D and C_L is confined to some selected blade profiles only [11-15]. Therefore, an inspection of C_D and C_L values of optimized profiles is on-demand to get a brief idea of the flow physics. As of now, C_D and C_L of a blade profile that is generated through the simplex search technique has not been reported open literature. In this ambiance, in the present investigation, 2D unsteady simulations are carried out for the optimized profile [16] adopting the SST k-ω turbulence model to examine the consequence of C_D and C_L of the blade profile. The total pressure, velocity magnitude, and turbulence intensity contours have been generated and probed. Further, simulations are performed for a semicircular profile in the similar environment to have a direct correlation between them.

2 DEVELOPMENT OF THE BLADE PROFILE

Fernando and Modi [17] carried out wind tunnel experiments to get the impact of performance parameters on the efficiency of a Savonius rotor. Fujisawa [18] came up with an idea to get the maximum C_P with *OR* as a performance variable. The study demonstrates a decrease of C_P with an increase of *OR*, showing the optimum *OR* to be 0.15. Gupta et al. [19] also found a maximum C_P of 0.25 at 20% overlap condition. Similarly, the C_P and C_T decreased with an increase of *OR* in the range of 0% to 16.2%. From wind tunnel experiments with several stages, Saha et al. [20] have found the 2-bladed system is optimum. They also obtained a higher C_P of the rotor with twisted blades as compared to a semicircular-bladed rotor. It was also shown that the 2-staged Savonius rotors have a better C_P as compared to 1- or 3-staged Savonius rotors. Moreover, Mahmoud [21] found that a 2-bladed rotor works much better than a 3-bladed rotor. It is reported that a Savonius rotor with end plates provides better performance than the ones without endplates. Jeon et al. [22] evaluated the effects of end plates on the operation of helical bladed wind turbines at 180° twist-angle. Apart from this, they studied a couple of other turbines with semicircular blades, and found the C_P to be proportional to the plate surface area. The use of end-plates in the Savonius rotor significantly increased the C_P by 36% as compared to those without end-plates.

Akwa et al. [23] performed computational analysis and their results were found to be consistent with test data [18, 19]. The highest turbine performance of this blade at *OR* = 0.15 gives an average C_P equal to 0.316 at *TSR* = 1.25. Roy and Saha [24] performed a 2D unsteady simulations to determine the effect of *OR* on the static torque characteristics and found a reduction of negative torque coefficient at *OR* = 0.20. This *OR* provided a low static torque variation at different turbine angular positions and also gave a higher mean static C_T as compared to the other *OR*s. Alom and Saha [25] tested elliptical-bladed profiles at various cut angles of $\theta = 45°$, 47.5°, 50°, and 55° and found that the elliptical profile with $\theta = 47.5°$ showed C_{Pmax} of 0.33 at *TSR* = 0.8, and the conventional semicircular profile showed a maximum C_{Pmax} of 0.27. Roy et al. [26] adopted a differential evolutionary algorithm, where an inverse optimization method is used for the optimization of the semicircular profile. This method brought a reduction of the swept area of the turbine by 9.8% for the given torque and power. Chan et al. [27] incorporated a computational fluid dynamics (CFD) model into the genetic

algorithm for numerical simulation of a conventional semicircular profile. Zhou et al. [28] investigated the potential of optimization technique on the geometry of a Savonius blade profile by using the evolutionary algorithm established on a 2D discrete cosine transformation (2D-DCT) using numerical simulation and improved the efficiency of the rotor by 13.77% at *TSR* = 1.0.

2.1 Optimization algorithm

In this study, the simplex serach method, one of the most popular direct search numerical optimization techniques, is taken for optimization [29]. This simplex search method was first discovered by George Bernard Dantzig in 1947 [30] to solve linear programming. The method starts by creating a non-zero volume hypercube/simplex using (N+1) points in an N-dimensional variable space. The objective function is then calculated at these points, and they are then categorized as the worst point (x_h), the best point (x_b), and next to the worst point (x_g). For the maximization problem, x_h is referred as a point that has the lowest objective function value. Likewise, x_b shows the maximum function value among the rest of the N points. Since this method is developed to move away from the worst point, the centroid (x_c) of all, but the worst point is calculated and x_h is reflected through x_c as $x_r = 2x_c - x_h$. The objective function is then calculated at the reflected point, x_r. If the objective function value of x_r is better than x_b, then the new point is further expanded as $x = (1+\gamma)x_c - \gamma x_h$, where γ is constant and its value is greater than one. In case x_r is worse than x_h, the new point is contracted as $x = (1-\beta)x_c + \beta x_h$, where β is another constant and its value lies between 0 and 1. If x_r is better than x_h, but worse than x_g, then the new point is contracted as $x = (1+\beta)x_c - \beta x_h$. The new point created by any of the above cases is then included in the simplex method by removing x_h. The procedure continues till a maximum number of iterations is reached or a difference between the new point and the best point is less than some smaller value ($\epsilon < 0.1\%$). The optimal value of the decision variables (x, y) is 75.4766 and 48.0479 respectively, and the corresponding C_T value is 0.328. For convergence meet, the overall mass, momentum, and energy balance are achieved. Apart from this, the residuals history is also monitored for seeking the convergence criteria which is found to be of order 10^{-5}. All these criteria are served to check if there is any unwanted driving potential to ensure the convergence of the solution.

2.2 Geometry of the tested profile

The dimensions of the tested blade profile have been shown in Figure 3. The oveall diameter *(D*) is taken as 200 mm. The *OR* for the semicircular and the optimized profiles is chosen to be 0.0.

2.3 Savonius rotor geometry

A conventional Savonius wind rotor with two identical semicircular blades is presented in Figure 4 along with other parameters. The chord length (L) of one semicircular blade is 100 mm with a homogeneous thickness (*t*) of 2 mm. The blades revolve regularly about the center (0,0) with a dimension (D = 2L) at an angular velocity ω_z. The two blades are separated by a spacing (*SG*) and an overlap (*OR*).

The x coordinate is set along with the incoming wind which is set at a velocity of V = 7.30 m/s [27]. The y coordinate is along the cross-stream direction. Therefore, the current work aims to analyze the aerodynamic coefficients of the optimized blade profile, therefore, the separation gap (*SG*) and overlap ratio (*OR*) are neglected, i.e, *SG* = *OR* = 0. The *TSR* is set at a constant value of 0.8 and the corresponding angular velocity is ω_z = 58.4 rad/s.

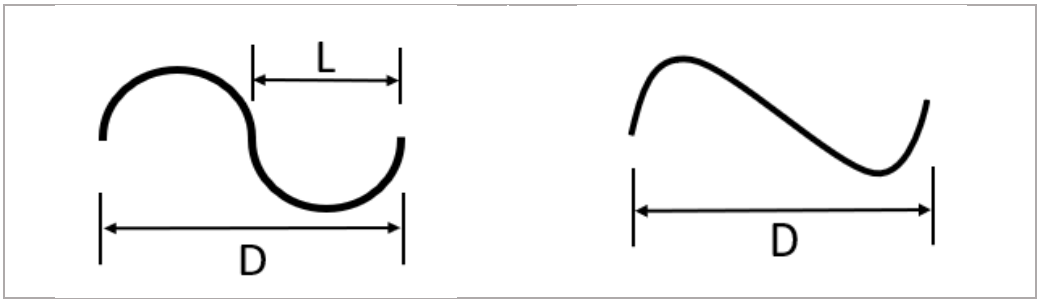

(a) Semicircular profile (b) Optimized profile

Figure 3: Dimensions of the tested blade profiles

2.4 Optimization Problem Formulation

The formulation of shape optimization of the blade profile of conventional Savonius wind turbine [27] is displayed in Figure 4.

$$\begin{aligned} &Maximize \\ &\quad C_T\,(x,y) \\ &subject\ to \\ &\quad 0<x<L\,,\ 0<y<0.75L \end{aligned} \tag{3}$$

Here, C_T is the time-averaged torque coefficient, and x and y are the coordinates of a point. Since two ends of the half of the blade are fixed, only one intermediate point is used to design the profile using a natural cubic spline curve. The coordinates x and y of the intermediate point thus become the design variable of the given optimization problem. The C_T is calculated using ANSYS ICEM CFD and ANSYS Fluent [31, 32]. The simplex search method is used with a bracket penalty function for optimizing the C_T value.

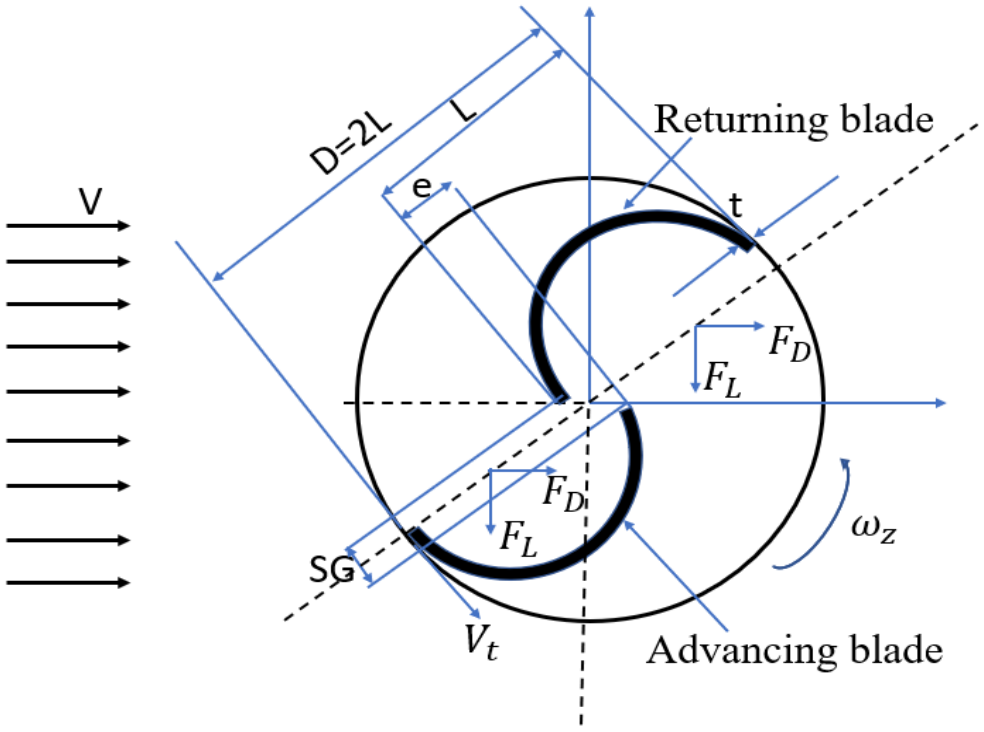

Figure 4: A typical semicircular-bladed Savonius rotor

2.5 Methodology

As depicted in Figure 5, the automated process is used for the blade depth formation that clubs the definition of the blade geometry, mesh generation and performance evaluation along with CFD simulations. The MATLAB is engaged as workflow analysis, calling all the coded systems in sequence. Since the number of decision variables is two, as per the simplex search method three random initial points need to be provided that lie within the search space. Each of these points is used with two other fixed points such as (0,0) and (*L*,0) to define one blade profile as shown in Figure 6. Now, a natural cubic spline is fitted using these two fixed points and one variable point. This gives a blade skeleton which is then given an offset value '*t*' to obtain the inner and outer surface points of the blade. All the points that lie on the surface of the blade are extracted and saved as a .txt file in a particular format. Similarly, the other two variable points chosen initially are used to provide two more blade geometries. Once the formatted data points are stored in the text file for the different blade geometries, the ANSYS ICEM CFD is launched. This software package is used to import all these data points to form the respective geometries. Once the geometry is imported, it can be meshed, and then the meshed file is stored in a format that is acceptable by ANSYS Fluent to carry out further simulations. The whole process can be recorded and saved into a script file for automating the whole geometry and meshing process. Now, the ANSYS Fluent is launched and the solution setup is given and simulations are carried out. The results are again saved into the text file. All the operations in the ANSYS Fluent are also recorded in a journal file to automate the process for future iterations. The text file carrying the results of the simulation is read by the MATLAB code and the time-averaged C_T obtained is the objective function value for the given problem. Then the simplex search method with a bracket operator penalty method is executed to generate new points. This process is carried out until the termination conditions are met. Once the final optimum blade shape is obtained, it is compared with the conventional semicircular rotor blade profile over a wide range of *TSR*.

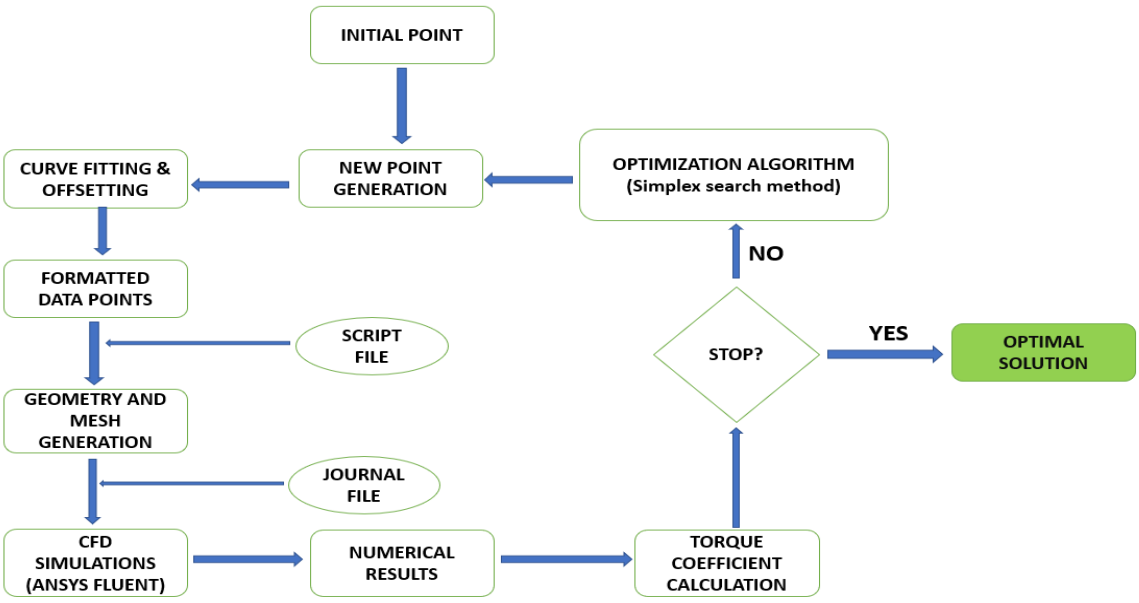

Figure 5: Process flow chart of simplex search method

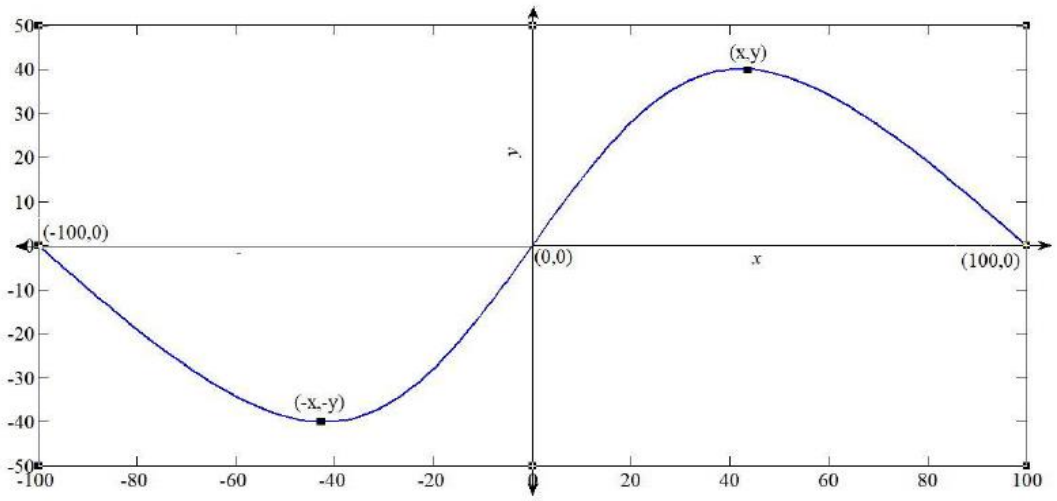

Figure 6: Blade skeleton with fixed and variable points

3 COMPUTATIONAL DOMAIN AND BOUNDARY CONDITIONS

The computational domain is illustrated in Figure 7. It is categorized into two parts, i.e., a rotating zone and a non-rotating zone. The rotational zone houses the turbine blades and the center coincides at the origin. The dimensions of the rotor blade are L, and the entire rotational zone is 2L. The non-rotational zone is a rectangle. The upper and lower horizontal edges are assigned at a distance of 7.5L from the origin and are given the part name 'Symmetry.' The left vertical edge (named as 'Inlet') is located at a distance of 7.5L before the origin, while the right vertical edge (named as 'Outlet,) is located at a gap of 15L against the origin [16]. The boundary conditions are the velocity inlet with 7.30 m/s and the pressure outlet with ambient condition. The turbulent intensity is kept within 1%. The upper and lower edges are given 'Symmetric' boundary condition. The blade surface is set to 'wall' and further moving wall, rotational motion, and no-slip conditions are selected. There is an interface between the two zones. The size of the outer space is selected in such a way that no boundary effect on the operation of the turbine is apparent. The diameter of the interface region is assigned 2*L* [16, 27].

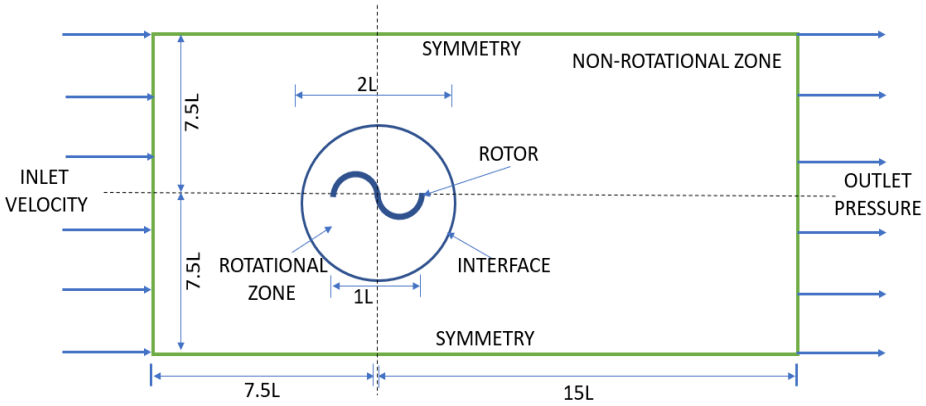

Figure 7: Computational domain and boundary conditions

4 NUMERICAL ASPECTS OF THE SIMULATION

This section includes meshing of the domain, grid independency test, implementation of the turbulence, and the solver structure as explained below.

4.1 Meshing

The unstructured mesh with all-tri elements is used throughout the domain. The sliding mesh option is used at the interface between the rotating and the non-rotating zones and is given a rotational speed of 58.4 rad/s correspondings to the *TSR* value of 0.8. Figure 8 displays the mesh image of the non-rotational zone, while Figure 9 shows the mesh image of the rotational zone at the boundary.

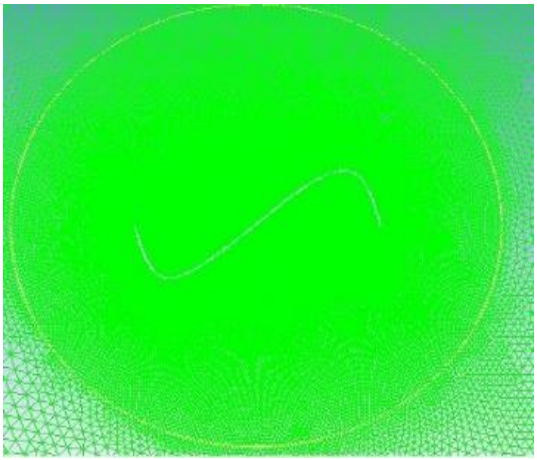

Figure 8: Nonrotational zone

4.2 Grid Independence Tests

The grid independence and time-independence examinations are accomplished for the conventional semicircular profile. The blade profile is generated using one of the optimum points (60.84, 35.65) [27], which is used to carry out the grid independence test. Three sets of mesh are tested, and the total number of elements in the three meshes varies from 65000 (mesh 1) to 100000 (mesh 2) and then to 140000 (mesh 3) [16]. The time-averaged C_T values at a constant time step of 2.988755×10^{-4} s for the three meshes are 0.2309, 0.2357, and 0.2363, and the corresponding time (in hours) required to complete the simulations is 4.25, 6, and 8.5. It can be seen that C_T increases by 2.07% from mesh 1 to mesh 2 and the enhancement in time taken is not more than 2 hours. From mesh 2 to mesh 3, the C_T increases by 0.25% while the time is taken to complete the simulation increases by 2.5 hours. Therefore, to save the computational effort, mesh 2 is selected in the present study (Table 1).

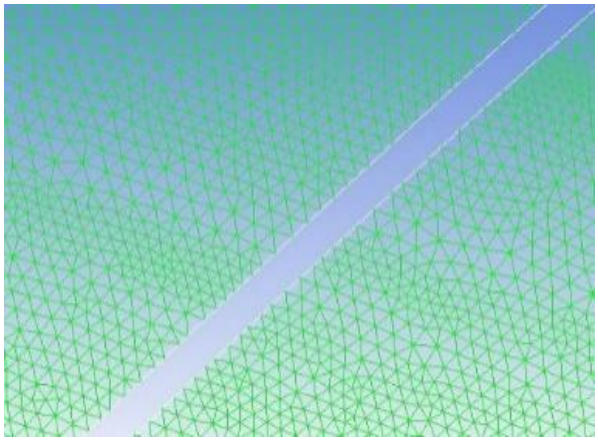

Figure 9: Rotational zone near the boundary

As stated earier, the boundary conditions are the velocity inlet with 7.30 m/s and the pressure outlet with ambient condition. Both the boundary conditions are limited to a turbulence level of 1% [14]. No-slip boundary condition is assigned at the interface between the rotational and the non-rotational zones. The upper and lower walls are taken as symmetry boundary conditions. The outflow near the turbine rotor is turbulent. Unsteady simulations have been taken into account to simulate the flow field. For each degree of rotation, the time step size has been chosen; accordingly, 23 iterations have been taken per unit time step. Five complete rotations are

taken to conduct the simulations. The simulation is stopped after reaching the convergence criteria of 10^{-5}. The second-order upwind scheme is adopted to discretize the temporal and the conservative term. For the pressure velocity coupling, a semi-implicit method for pressure linked equations (*SIMPLE)* is chosen for better stability of the solution. The *SST k-ω* model is adopted to simulate the flow field due to its better prediction capability [23, 33-35].

Table 1: Grid independency test

Mesh	No. of meshing elements	C_T	Time (hours)
1	65000	0.2309	4.25
2	100000	0.2357	6
3	140000	0.2363	8.5

4.3 Turbulence Model

A finite volume method-based solver, ANSYS Fluent is adopted to solve the unsteady Reynolds-averaged Navier-Stokes (RANS) equation to conduct 2D transient simulations. The turbulent viscosity term in the RANS equation is calculated using the shear-stress transport (SST) *k-ω* turbulence model. The SST *k-ω* turbulence model associates the benefits of both *k-ε* model for the free stream cascades and the *k-ω* model for the boundary layer cascades to ensure that the flow separation with adverse pressure gradients is predicted accurately [23, 33-35].

4.4 Solver setup

The second order upwind scheme is used for the spatial discretization, kinetic energy, and a certain degree of distribution. The second-order pattern is adopted for pressure while the least square pattern is adopted for the gradient. The SIMPLE system is used for pressure velocity coupling.

5 VALIDATION OF RESULTS

The SST *k-ω* turbulence model is adopted to conduct the 2D unsteady simulations for the current study at an inlet air speed of 7.3 m/s depending upon the diameter of the rotor (*L*). The consequences of present 2D unsteady simulations are compared with existing data of Roy and Ducoin [14], who performed the simulation at R_e = 1.23x10^5 for the conventional semicircular profile as shown in Figure 10. The investigation is accomplished at *TSR* = 0.6 as well to validate the result with Roy and Ducoin [14]. The average C_D for the entire rotor replacement is almost identical. The C_{Davg} is found to be 1.19 in the present investigation.

The showcase of instantaneous C_L values for a complete revolution is shown in Figure 11. It is observed that the semicircular profile used in the present study shows the C_{Lavg} of 1.06 as compared to the C_{Lavg} of 0.85 as reported by Roy and Ducoin [14]. Thus, the optimized profile shows a little over prediction because of 2D simulations, and this could be overcome if 3D simulations are conducted.

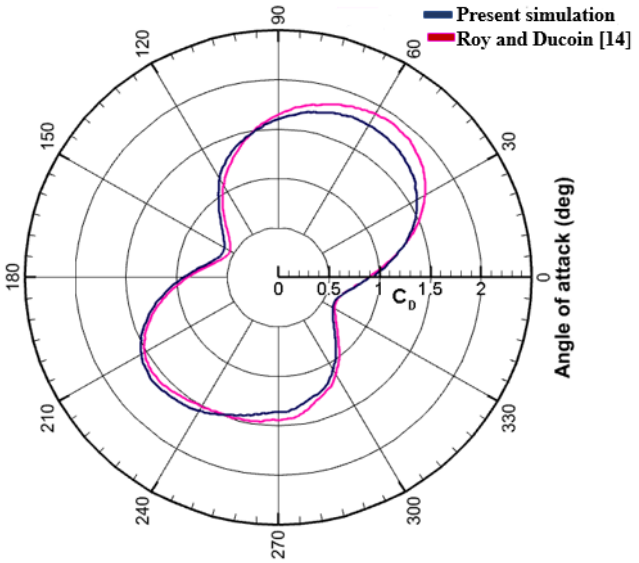

Figure 10: C_D of the semicircular profile

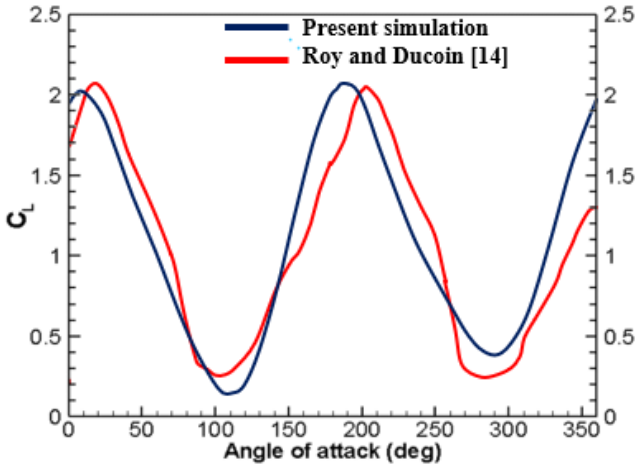

Figure 11: C_L of the semicircular profile

6 RESULTS AND DISCUSSION

The 2D unsteady simulations are performed for an optimized blade profile and for a conventional semicircular blade profile. Simulations are accomplished for optimized profile and semicircular profile under similar circumstances. Figures 12 and 13 show a deviation of C_D and $C_{L,}$ respectively for both the profiles. The C_{Dmax} for the optimized profile is found to be 1.91 at α = 54° and the C_{Dmin} of the same profile is 0.45 at α = 147°. While the semicircular profile shows C_{Dmax} of 1.78 at α = 60°, and the C_{Dmin} of 0.60 at α = 154° and 334°. Thus, it can be seen that the optimized profile shows an increment in C_{Dmax} of around 7.3%. On the other hand, the C_{Lmax} of the optimized profile is found to be 2.11 at α = 53°, while the C_{Lmax} of semicircular profile is seen to be 2.13, demonstrating the inferiority of the optimized profile. The optimized profile thus has demonstrated its improved performance in terms of C_{Dmax} as compared to the conventional semicircular profile. In the present study, total pressure, velocity magnitude, and turbulence intensity contours are generated at different α, however, for the sake of understanding, limited results are depicted in Figures 14 through 16.

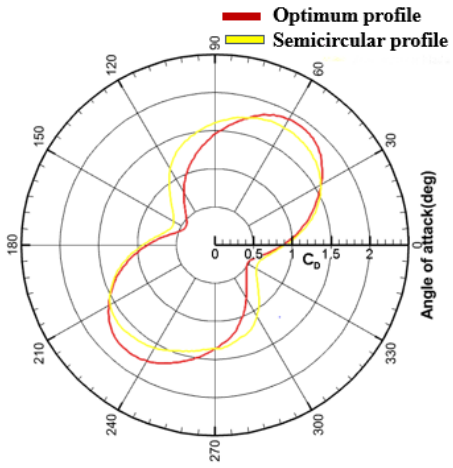

Figure 12: C_D of the optimized and semicircular profile at *TSR* = 0.8

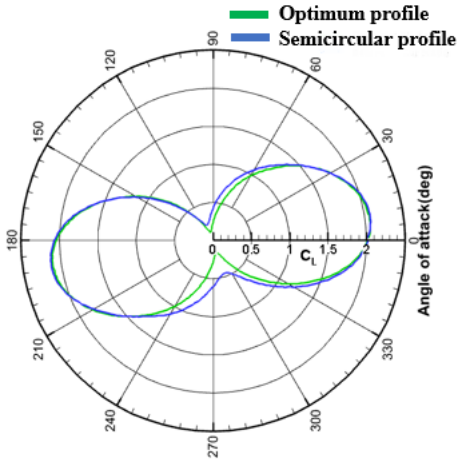

Figure 13: C_L of the optimized and semicircular profile at *TSR* = 0.8

6.1 Pressure Contours

Figure 14 displays the total pressure contours of the optimum and the semicircular profiles at *TSR* = 0.8. The total pressure around the advancing blade of an optimized profile and semicircular profiles ranges between 0 to 40 N/m^2, and –40 to 60 N/m^2. Moreover, the flow separation is also delayed for the optimized blade as compared to the semicircular profile. Therefore, the pressure recovery is improved at the blade boundary, resulting a higher C_{Dmax} for the optimized profile. This is the reason behind the improved performance of the optimized profile.

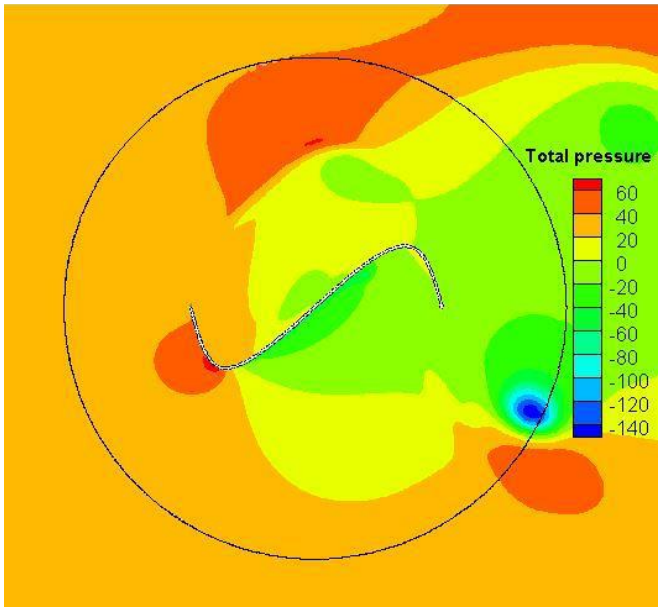

(a) Optimum profile at $\alpha = 0^0$

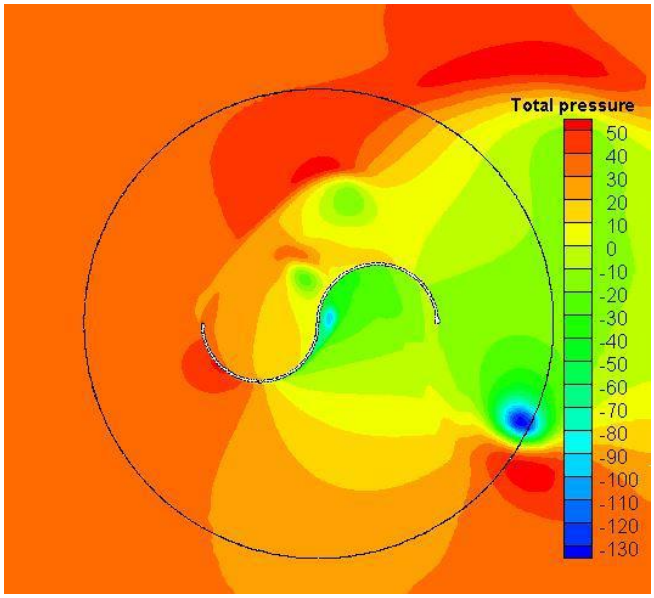

(b) Semicircular profile at $\alpha = 0^0$

Figure 14: Total pressure (N/m^2) contours of the tested profile at *TSR* = 0.8

6.2 Velocity Contours

Figure 15 shows the velocity magnitude contours of the optimum and the semicircular profiles at *TSR* = 0.8. On the concave region of the advancing blade, the velocity magnitude of the optimum profile ranges between 3 to 6 m/s, while for the semicircular profile, it ranges between 1 to 4 m/s. On the other hand, the convex region of the advancing blade, the velocity magnitude for the optimum profile ranges between 8 to 17 m/s; while for the semicircular profiles, it ranges between 7 to 15 m/s essentially covering a much larger area than the optimized blade.

The advancing blade of the optimized profile thus experiences much lesser negative drag than on the semicircular profile. Now, for the returning blade, the velocity magnitude on the concave side of the optimized profile is more against the semicircular profile, and the velocity magnitude on the convex side is again much lesser than that of the semicircular profile. This again ensures that the negative drag on the returning blade is lesser for the optimized profile in comparison to the semicircular profile. Since the Savonius rotor is driven by a drag force, the lesser value of the negative drag helps to obtain a higher C_T value, which in turn improves the rotor performance.

6.3 Turbulence Intensity Contours

Figure 16 displays the turbulent intensity contours of the optimized and the semicircular profiles at *TSR* = 0.8. The magnitude of turbulence intensity range from 0 to 0.16 for the optimized profile, while it varies from 0 to 0.22 for the semicircular profile. It can also be noted that in a semicircular profile, the turbulence intensity is higher at the downstream, which can lead to the generation of the vortex and reduces the performance of the rotor.

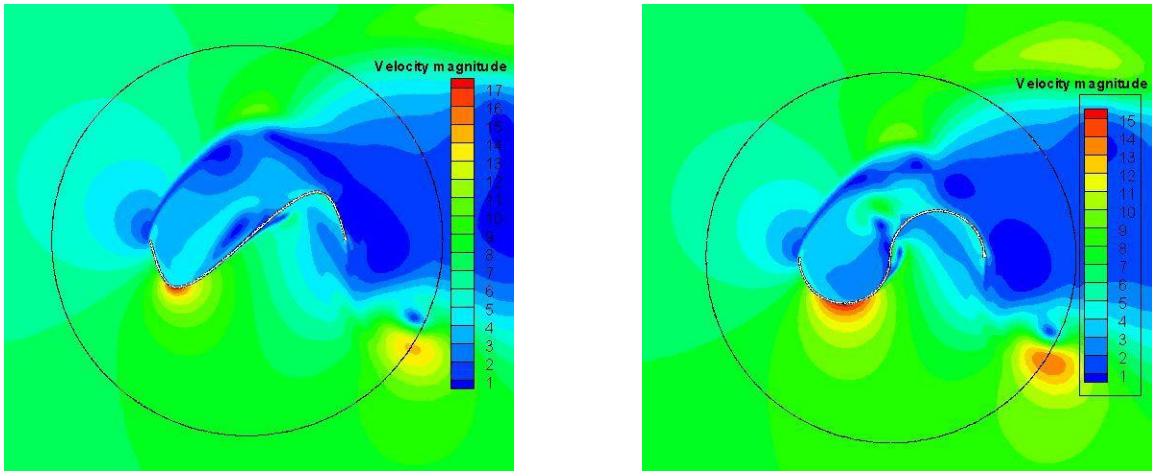

(a) Optimum profile at $\alpha = 0^0$ (b) Semicircular profile at $\alpha = 0^0$

Figure 15: Velocity magnitude (m/s) contours of the tested profile at *TSR* = 0.8

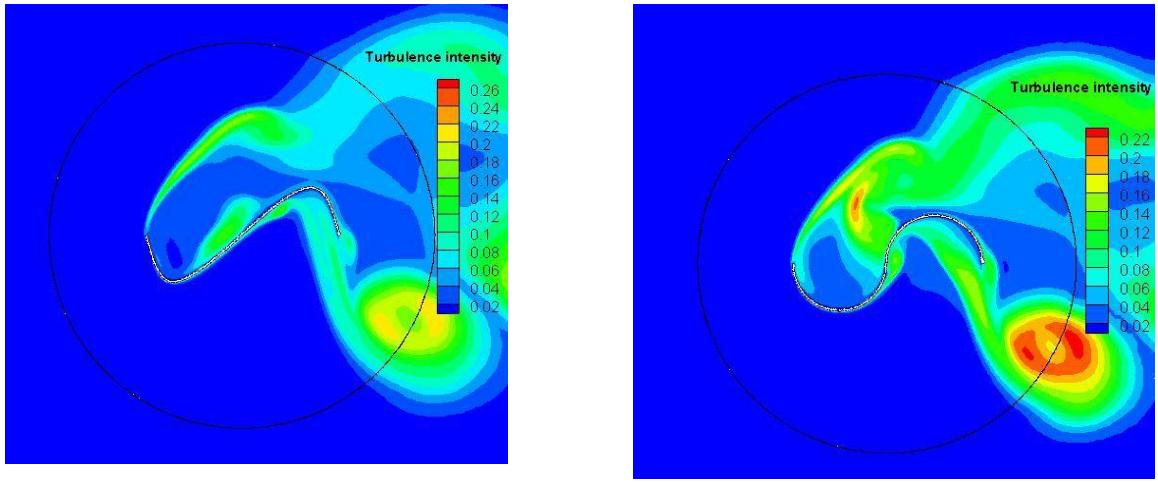

(a) Optimum profile at $\alpha = 0^0$ (b) Semicircular profile at $\alpha = 0^0$

Figure 16: Turbulence intensity (%) contours of the tested profile at *TSR* = 0.8

7 CONCLUSIONS

The Savonius rotor, a type of VAWT, is mainly driven by the drag force acting on the blade. This type of turbine is very effective in small-scale power production in remote and inaccessible areas. In the present study, the aerodynamic coefficients (C_D and C_L) of an optimized blade profile developed through the simplex search method is studied. In this regard, 2D unsteady simulations are accomplished for the optimized profile using the SST k-ω turbulence model. For the sake of comparison, 2D unsteady simulations of the conventional semicircular profile are also carried out under identical conditions. From the study, the C_{Dmax} of the optimized profile is found to be 1.91, while for the semicircular profile it is found to be 1.78. This shows an increment of 7.3% for the optimized profile. Moreover, both the them shows similar C_L values and the C_{Lavg} is found to be 1.07. The velocity magnitude and the total pressure obtained are higher in the vicinity of the advancing side of the optimized profile, while the turbulence intensity is found to be lesser as compared to the semicircular profile. The over prediction in the value of C_L as compared to the work reported in literature can be eliminated by adopting a 3D simulation. As a future scope of study, the local drag coefficient can be analysed to get the variation of C_D and C_L values throughout the blade region at any point of coordinates.

REFERENCES

[1] Singh, R. K., and Ahmed, M. R., 2013, "Blade Design and Performance Testing of a Small Wind Turbine Rotor for Low Wind Speed Applications," Renewable Energy, 50, pp. 812-819.

[2] Boontome, P., Therdyothin, A., and Chontanawat, J., 2017, "Investigating the Causal Relationship Between Non-Renewable and Renewable Energy Consumption, CO_2 Emissions and Economic Growth in Thailand," Energy Procedia, 138, pp. 925-930.

[3] Amano, R. S., 2017, "Review of Wind Turbine Research in 21st Century," ASME Journal of Energy Resources Technology, 139(5), p. 50801.

[4] Alom, N., and Saha, U. K., 2018, "Performance Evaluation of Vent-Augmented Elliptical-bladed Savonius Rotors by Numerical Simulation and Wind Tunnel Experiments," Energy, 152, pp. 277-290.

[5] Alom, N., and Saha, U. K., 2017 "Arriving at the Optimum Overlap Ratio for an Elliptical-Bladed Savonius Rotor," in Proceedings of ASME Turbo Expo Turbine Technical Conference and Exposition, June 26–30, Charlotte, North Carolina, USA.

[6] Alom, N., Kolaparthi, S. C., Gadde, S. C., and Saha, U. K., 2016, "Aerodynamic Design Optimization of Elliptical-Bladed Savonius-Style Wind Turbine by Numerical Simulations," Paper No. OMAE2016-55095, ASME 35th International Conference on Ocean, Offshore and Arctic Engineering, June 19–24, Busan, South Korea.

[7] Alexander, A. J., and Holownia, B. P., 1978, "Wind Tunnel Tests on a Savonius Rotor," Journal of Industrial Aerodynamics, 3, pp 343–51.

[8] Alom, N., and Saha, U. K., 2018, "Four Decades of Research into the Augmentation Techniques of Savonius wind Turbine Rotor," ASME Journal of Energy Resources Technology, 140(5), p. 050801.

[9] Manwell, J. F., Mcgowan J. G., and Rogers, A. L., 2009, "Wind Energy Explained: Theory, Design, and Application," UK: John Wiley & Sons Limited.

[10] Roy, S., and Saha, U. K., 2013, "Review of Experimental Investigations into the Design, Performance, and Optimization of the Savonius Rotor," Proc. Inst. Mech. Eng. Part A-Journal Power Energy, 227(4): pp 528–542.

[11] Chauvin, A., and Benghrib, D., 1989, "Drag and Lift Coefficients Evolution of a Savonius Rotor," Experiments in Fluids, 8(1-2), pp. 118-20.

[12] Irabu, K., and Roy, J. N., 2011 "Study of Direct Force Measurement and Characteristics on Blades of Savonius Rotor at Static State," Experimental Thermal and Fluid Science, 35(4): pp. 653–659.

[13] Jaohindy, P., McTavish, S., Garde, F., and Bastide, A., 2013 "An Analysis of the Transient Forces Acting on Savonius Rotors with Different Aspect Ratios," Renewable Energy, 55, pp. 286-295.

[14] Roy, S., and Ducoin, A., 2016 "Unsteady Analysis on the Instantaneous Forces and Moment Arms Acting on a Novel Savonius-Style Wind Turbine," Energy Conversion and Management, 121, pp. 281–296.

[15] Alom, N., Borah, B., and Saha, U. K., 2018. "An Insight into the Drag and Lift Characteristics of Modified Bach and Benesh Profiles of Savonius Rotor," 4th International Symposium on Hydrogen Energy, Renewable Energy and Materials (HEREM), June 13–14, Bangkok, Thailand.

[16] Agrawal, A., Kansagara, D., Sharma, D. S., Saha, U. K., 2019, "Savonius Wind Turbine Blade Profile Optimization by Coupling CFD Simulations with Simplex Search Technique," Paper No. GTINDIA2019-2442, Proceedings of the ASME 2019 Gas Turbine India, December 5-6, Chennai, Tamil Nadu, India.

[17] Modi, V. J., and Fernando, M. S. U. K., 1989, "On the Performance of the Savonius Wind Turbine," ASME Journal of Solar Energy Engineering, vol. 111, no. 1, p. 71.

[18] Fujisawa, N., 1992, "On the Torque mechanism of Savonius Rotors," Journal of Wind Engineering and Industrial Aerodynamics, vol. 40, no. 3, pp. 277–292.

[19] Gupta, R., Biswas, A., and Sharma, K. K., 2008, "Comparative Study of a Three-bucket Savonius Rotor with a Combined Three-bucket Savonius three-bladed Darrieus Rotor," Renewable Energy, vol. 33, no. 9, pp. 1974–1981.

[20] Saha, U. K., Thotla, S., and Maity, D., 2008, "Optimum Design Configuration of Savonius Rotor Through Wind Tunnel Experiments," Journal of Wind Engineering and Industrial Aerodynamics, vol. 96, no. 8–9, pp. 1359–1375.

[21] Mahmoud, N. H., El-Haroun, A. A., Wahba, E., and Nasef, M. H., 2012, "An Experimental Study on Improvement of Savonius Rotor Performance," Alexandria Engineering Journal, vol. 51, no. 1, pp. 19–25.

[22] Jeon, K. S., Jeong, J. I., Pan, J. K., and Ryu, K. W., 2015, "Effects of End Plates with Various Shapes and Sizes on Helical Savonius Wind Turbines," Renewable Energy, vol. 79, no. 1, pp. 167–176.

[23] Akwa, J. V., Junior, A. S., G and Petry, A. P., 2012 "Discussion on the Verification of the Overlap Ratio Influence on Performance Coefficients of a Savonius Wind Rotor using Computational Fluid Dynamics," Renewable Energy, 38(033109): pp 141-149.

[24] Roy, S., and Saha, U. K., 2013, "Computational Study to Assess the Influence of Overlap Ratio on Static Torque Characteristics of a Vertical Axis Wind Turbine," Procedia Engineering, vol. 51, pp. 694–702.

[25] Alom, N., and Saha, U. K., 2018, "Performance Evaluation of Vent-augmented Elliptical-bladed Savonius Rotors by Numerical Simulation and Wind Tunnel Experiments," Energy, vol. 152, pp. 277–290.

[26] Roy, S., Das, R., and Saha, U. K., 2018, "An Inverse Method for Optimization of Geometric Parameters of a Savonius-style Wind Turbine," Energy Conversion and Management, vol. 155, pp. 116–127.

[27] Chan, C. M., Bai, H. L., and He, D. Q., 2018. "Blade Shape Optimization of the Savonius Wind Turbine using a Genetic Algorithm," Applied Energy", 213, pp. 148–157.

[28] Zhou, Q., Xu, Z., Cheng, S., Huang, Y., and Xiao, J., 2018, "Innovative Savonius Rotors Evolved by Genetic Algorithm Based on 2D-DCT Encoding," Soft Computing, no. 2016, pp. 1–10.

[29] Ravindran, A., Ragsdell, K. M., and Reklaitis, G. V., 2006, "Engineering Optimization: Methods and Applications," Wiley Publications, 2nd edition.

[30] Dantzig, G. B., and Thapa, M. N., 1997, "Linear Programming 1: Introduction, Springer-Verlog, New York.

[31] ANSYS Inc, 2009. ANSYS Fluent Theory Guide 12.0.

[32] ANSYS Inc, 2015. ANSYS Fluent Theory Guide 12.0.

[33] Talukdar, P. K., Sardar, A., Kulkarni, V., and Saha, U. K., 2018 "Parametric Analysis of Model Savonius Hydrokinetic Turbines Through Experimental and Computational Investigations," Energy Conversion and Management, 158, pp 36–49.

[34] Song, C., Zheng, Y., Zhao, Z., Zhang, Y., C. Li, and H. Jiang., 2015 "Investigation of Meshing Strategies and Turbulence Models of Computational Fluid Dynamics Simulations of Vertical Axis wind Turbines," Journal of Renewable and Sustainable Energy, 7: pp 0–19.

[35] Alom, N., Saha, U. K., and Dewan, A., 2021, "In the Quest of an Appropriate Turbulence Model for Analyzing the Aerodynamics of a Conventional Savonius (S-type) Wind Rotor," Journal of Renewable and Sustainable Energy, Vol. 13, Issue 2, p. 023313.

